Article

Not peer-reviewed version

Severe Plastic Deformation Significantly Enhances Strengthening and Toughening Effect of T6 Treated 7046 Aluminum Alloy

Yuna Wu *, Hongchen Dong, Hao Huang, Ting Yuan, Jing Bai, Jinghua Jiang, Feng Fang *, Aibin Ma

Posted Date: 22 August 2024

doi: 10.20944/preprints202408.1587.v1

Keywords: ECAP; Rolling; T6; Aluminum alloy; Strengthening and toughening

 doi:10.20944/preprints202408.1587.v1

Article

Severe Plastic Deformation Significantly Enhances Strengthening and Toughening Effect of T6 Treated 7046 Aluminum Alloy

Yuna Wu [1,2], Hongchen Dong [1], Hao Huang [1,2], Ting Yuan [3], Jing Bai [4], Jinghua Jiang [1], Feng Fang [4,*] and Aibin Ma [1]

[1] College of Materials Science and Engineering, Hohai University, Changzhou 213200, China
[2] Suqian Research Institute, Hohai University, Suqian 223800, China; www.dlamen@foxmail.com
[3] School of Chemistry and Materials Engineering, Changshu Institute of Technology, Changshu 215500, China; rabbityt@163.com
[4] School of Materials Science and Engineering, Southeast University, Nanjing 211189, China
* Correspondence: wuyuna@hhu.edu.cn (Yuna Wu); fangfeng@seu.edu.cn (Feng Fang)

Abstract: 7046 aluminum alloy has good fatigue property, corrosion resistance and weld property, but the moderate strength and plasticity limit its wider application and development. In the present study, severe plastic deformation (SPD) was applied prior to T6 treatment to significantly strengthen and toughen the 7046 aluminum alloy. Results indicate that the alloy processed by 4 passes of equal channel angular pressing (ECAP) at 300 ℃ prior to T6 treatment exhibits an excellent mechanical performance, with ultimate tensile strength (UTS) and elongation (EL) of 485 MPa and 19%, exhibiting an improvement of 18.6% and 375% compared to that of the T6 alloy, respectively. The mechanical properties of the alloy are further improved by the additional room temperature (RT) rolling process, with UTS of 508 MPa and EL of 23.4%. There are more precipitates of η' and Al6Mn phases in the 300℃4P-R80%-T6 and 300°C4P-T6 alloys, which contribute to the strengthening and toughening enhancement by SPD processed T6 alloy. The results of this work may shed some light on enhancing 7046 aluminum alloy.

Keywords: ECAP; Rolling; T6; Aluminum alloy; Strengthening and toughening

1. Introduction

7xxx series (Al-Zn-Mg-Cu) aluminum alloys are typical precipitate-reinforced alloys with high specific strength, good fracture toughness, excellent machining performance [1,2]. They are widely used in aerospace, advanced equipment manufacturing, rail transit, 5G applications and new infrastructure [3,4]. However, the service problems in the harsh and complex environment and the high-quality connection requirements between different materials in actual applications put forward higher requirements on the fatigue properties, corrosion resistance and weld properties of 7xxx series aluminum alloys [5,6]. Therefore, new Cu-free 7xxx series aluminum alloys containing small amounts of Zr and Ti (such as 7046) are investigated as promising candidates [7,8]. Studies concerning 7046 aluminum alloy mainly focus on its mechanical properties [9–11], fatigue property [8,12], corrosion resistance [10,13,14], and weld property [15,16], However, scant attention is placed on the strengthening and toughening mechanisms. Therefore, it is of great significance to further explore effective processing technologies for producing more strengthening and toughening 7046 aluminum alloys and gain a better understanding of the corresponding mechanisms.

Solid solution with peak aging (T6 treatment) is a common method to improve the strength of 7xxx aluminum alloys [17,18]. After T6 treatment, the GP zones precipitated in large quantities in grains can be transformed into η′ (MgZn2) phases. The coherent GP zones and semi-coherent η′ phases can cause severe lattice distortion and strengthen the alloy [19]. For example, an approximate 115 MPa increment in ultimate tensile strength (UTS) can be achieved in a 7A99 aluminum alloy processed by T6 treatment [20]. Both ultrafine-grained (UFG) and coarse-grained (CG) 7075 alloys

 doi:10.20944/preprints202408.1587.v1

exhibit a considerable increase in UTS after T6 treatment (the increment of them is about 143 MPa and 223 MPa respectively) [21]. Similar studies also have indicated that T6 treatment can obviously improve the strength of the alloys, but the increment is limited and always accompanied with strength-ductility trade off [22,23]. Thus, it is urgent to develop new processing technologies to echo the call for developing super higher-performance (high-strength and high-ductility) alloys.

To solve this problem, some researchers put forward applying room temperature (RT) severe plastic deformation (SPD) during T6 treatment (before aging and after solid solution treatment) to improve the comprehensive mechanical properties of the 7xxx aluminum alloys [24–26]. Studies indicate that 1 pass RT equal channel angular pressing (ECAP) after solid solution greatly shortens the peak-aging time of experimental 7055 aluminum alloy extrusion bars. The UTS and YS (yield strength) are improved 39 MPa and 33 MPa respectively, and the elongation (EL) remains around 9% compared with that of T6 treatment [27]. The UTS of Al-6.6Zn-1.96Mg-2.35Cu alloy subjected to 2 passes of cross accumulative extrusion bonding (CAEB) after solid solution treatment (470 ℃ for 1 h) and before aging (120 ℃ for 24 h) is 562 MPa, which is 40% more than that of T6 treated alloy. At the same time, the alloy can remain a good EL of 21.5% [28]. By embedding RT SPD process in solid solution and aging (T6 treatment), the grains of the alloys are easier to become finer because of the shear strain and the resultant recrystallization, which contributes to the fine-grain strengthening. Besides, more grain and subgrain boundaries formed during RT SPD provide more nucleation sites for the η′ phases, which enhances the precipitation strengthening [29–31].

The above-mentioned method (embedding RT SPD in T6 treatment) is effective in the easy-deformable 7xxx series aluminum alloys. However, some 7xxx series aluminum alloys with low plasticity (such as 7046 alloy) need to be SPD treated in high temperature (HT) [32,33]. It should be pointed out, dynamic precipitation would be significantly accelerated by the HT SPD [34], which means the GP zones and η′ strengthening phases would easily be transformed into η phases [34,35]. The strengthening effect of η phases is weak, thus this simple HT SPD process often doesn't play a role in the strengthening and toughening of the alloys. Therefore, some studies attempt to reperform T6 treatment after HT SPD. For example, 7055 aluminum alloy processed by two-stage solution treatment (470 ℃ for 16 h and 475 ℃ for 8 h), a double step hot rolling (250 ℃ for 20% reduction and 430 ℃ for 75% reduction) combined with T6 treatment shows excellent comprehensive mechanical properties. It exhibits a UTS, YS and EL of 610 MPa, 542 MPa and 21.6% respectively [36]. The successful attempt is inspirational for the simultaneous strengthening and toughening of hard-deformable 7xxx series aluminum alloys. But so far, few studies have paid attention to why the SPD process can enhance the strengthening and toughening effect of T6 treatment, let alone in 7046 alloys. In this study, 7046 aluminum alloy subjected to solid solution, HT SPD and T6 treatment is studied. It is demonstrated that HT ECAP combined with RT rolling enhance the strengthening and toughening effect of T6 treatment on 7046 aluminum alloy. By observing the microstructure of the alloys, the mechanism of increasing strength and ductility is discussed.

2. Experimental Material and Procedures

The as-cast 7046 aluminum alloys studied in this paper were specially customized, and the actual chemical composition was obtained by model ARL-3460 direct reading spectrometer, as shown in Table 1.

Table 1. Actual chemical composition of the 7046 alloy (wt.%).

Zn	Mg	Mn	Cu	Cr	Ti	Zr	Fe	Si	Al
7.26	1.7	0.26	0.22	0.01	0.02	0.13	0.14	0.09	Bal.

The cast alloy cut into samples with a size of 19.5 mm × 19.5 mm × 45 mm was solution-treated at 470 ℃ for 1 h and quenched in water. As 7046 alloys can hardly be ECAPed at RT, the ECAP die was heated to 300 ℃ by a resistance furnace and maintained for 1 h before inserting a sample into the entrance channel [37]. In order to avoid crack formation, all the samples have been ECAPed by 4 passes quickly and continually. ECAP was conducted with route Bc in a 90° die [38,39]. Cut out

 doi:10.20944/preprints202408.1587.v1

different thicknesses of sheets from 4P-ECAP samples along the extrusion direction. The sheets were rolled with a 5% average reduction per pass at RT, and the total reduction was 80%. Finally, all these samples were heat treated by T6 treatment (solid solution at 470 ℃ for 1 h and further aging at 120 ℃ for 24 h). These samples are named as 300℃4P-T6 and 300℃4P-R80%-T6 respectively. In addition, the as-cast, T6 and R80%-T6 samples were prepared for performance comparison.

Tensile tests were conducted to evaluate the mechanical properties of all samples. Tensile tests were carried out at RT using a universal testing machine (Suns-UTM4294X) at a loading speed of 0.5 mm/min. The microstructures of the alloys were characterized by optical microscopy (OM, BX6OM), transmission electron microscopy (TEM, FEI Tecnai G2 F20 S-TWIN) and electron backscatter diffractions (EBSD, Hitachi S-3400N). For OM observations, samples were ground by SiC abrasive papers, polished by 3.5 μm diamond spray, and finally etched by Keller's reagent for 75 s. EBSD samples were electropolished in the electrolytic polishing solution (10% HClO4 + 90% C2H5OH). The temperature was set to about -20℃, the voltage was constant at 32V, and the duration was 60s. For TEM observations, samples were firstly ground to approximately 60 μm by SiC abrasive papers and then thinned in an ion thinning apparatus (GATAN-691).

3. Results

3.1. Microstructure Observation

Figure 1 shows the optical microstructures of the as-cast, T6, 300℃-4P-T6 and 300℃-4P-R80%-T6 7046 alloys. As can be seen, the as-cast alloy is mainly composed of α-Al matrix and a small amount of second phases distributed along the grain boundaries (Figure 1a). These second phases mainly consist of primary MgZn2 phases and Al7Cu2Fe phases [40]. After T6 treatment, most of the MgZn2 phases dissolve into Al matrix, in addition to insoluble Al7Cu2Fe phases, only a small number of larger MgZn2 phases still remain, as shown in Figure 1b. Performing ECAP, ECAP and RT rolling before T6 treatment, the grain size of the alloy is obviously refined, and the originally coarse second phases become fine and dispersed, as shown in Figure 1c,d.

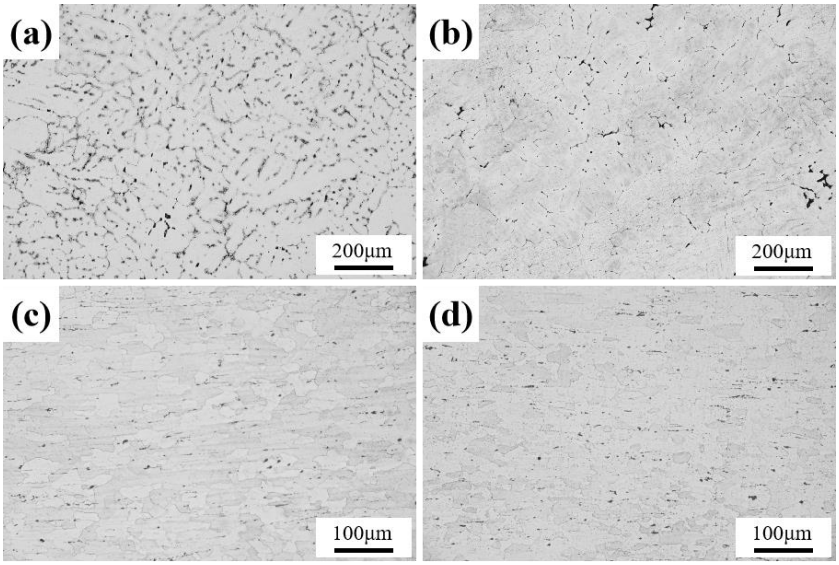

Figure 1. OM images of 7046 alloy: (a) as-cast; (b) T6; (c) 300℃4P-T6; (d) 300℃4P-R80%-T6.

Figure 2 exhibits the EBSD maps and grain size distribution of the as-cast, T6, 300℃-4P-T6 and 300℃-4P-R80%-T6 alloys respectively. The grain size distribution of the as-cast alloy is relatively homogeneous and the grains are nearly equiaxed (Figure 2a). The average grain size (AGS) of the as-cast alloy is approximately 241 μm as can be seen in Figure 2b. After T6 treatment, the grains grew slightly (Figure 2c) and the AGS is approximately 265 μm (Figure 2d). The grains still retained their elongated state when subjected to 4 passes of ECAP at 300 ℃ combined with T6 treatment, with most of the grains becoming fine recrystallized grains (as shown in Figure 2e). The AGS of 300℃-4P-

 doi:10.20944/preprints202408.1587.v1

T6 alloy reduced to 40 μm (Figure 2f). With the additional RT rolling process after ECAP and before T6 treatment, the grain size of the alloy was further refined, the elongated state of the grains is weakened and almost all of the grains become fine recrystallized grains (Figure 2g). The AGS of 300 ℃-4P-R80%-T6 alloy further reduced to 19 μm (Figure 2h).

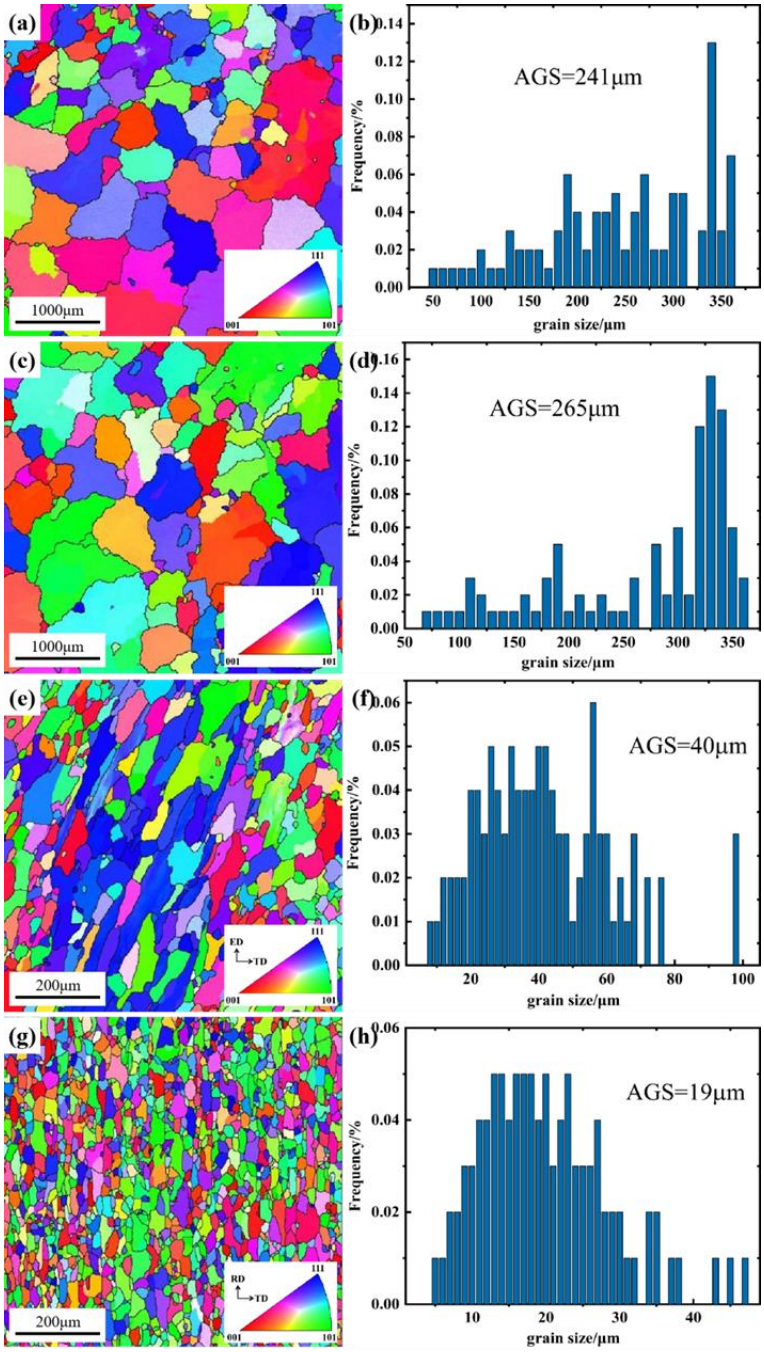

Figure 2. EBSD maps of 7046 alloy: (a, c, e, g) OIM maps; (b, d, f, h) grain size distribution; (a, b) as-cast; (c, d) T6; (e, f) 300℃4P-T6; (g, h) 300℃4P-R80%-T6.

Figure 3 visualizes the polar figures of T6, 300℃4P-T6 and 300℃4P-R80%-T6 alloy respectively. As shown in Figure 3a, the peak texture intensity of T6 alloy is 5.41. Performing ECAP extrusion prior to T6 treatment, the peak texture intensity of the alloy decreases slightly to 5.31 (Figure 3b). Performing ECAP and RT rolling prior to T6 treatment, the peak texture intensity of the alloy is further weakened to 3.02 (Figure 3c) with a more uniform weave distribution.

 doi:10.20944/preprints202408.1587.v1

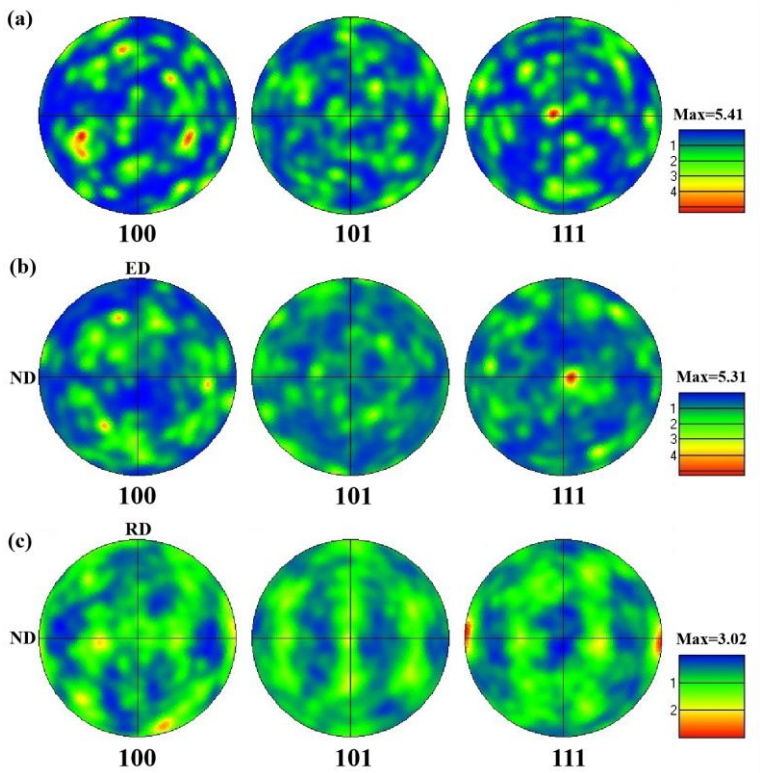

Figure 3. Pole figures on the RD/ED-ND cross-section of (a) T6, (b) 300℃4P-T6 and (c) 300℃4P-R80%-T6.

As all the samples after different processes were subjected to T6 treatment, the dislocation intensity in the samples is rather low, so the precipitates are paid more attention. Figure 4 illustrates the three typical precipitates distributed along the grain boundaries and inside the grains of T6 alloy observed by TEM. Firstly, as shown in Figure 4a,b, the η phases with a large dimensional difference are observed along the grain boundaries in T6 alloy, with length dimensions ranging from approximately 30 nm to 450 nm and length-diameter ratios ranging from 1.6 to 5.1. Precipitate free zone (PFZ) with a width between 120 nm and 180 nm is found at the grain boundaries of the alloys. Secondly, a lot of biggish short rod-like Al6Mn phases (its average length is about 102 nm, and length-diameter ratio is about 2.6) are distributed inside the grains (Figure 4c). Finally, as shown in Figure 4c,d, a large number of small oval η′ phases (its size is about 5 nm) are diffusely distributed in the grains.

 doi:10.20944/preprints202408.1587.v1

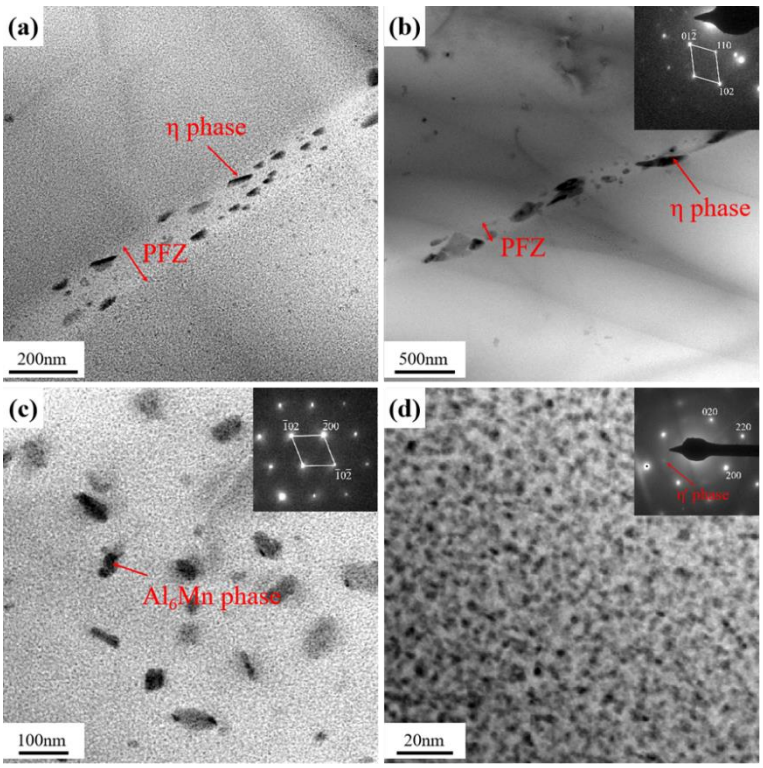

Figure 4. Typical precipitates of T6 alloy observed by TEM: (a, b) along grain boundaries; (c, d) inside grains.

Figure 5 presents the three typical precipitates in 300℃4P-T6 alloy. As compared Figure 5a with Figure 4a,b, the size distribution of the η phases at the grain boundaries of 300℃4P-T6 alloy is more uniform and finer than that of T6 alloy, with an average length of about 38 nm and a length-diameter ratio of about 2.7. The width of the PFZ at the grain boundaries is significantly reduced to 44 nm (Figure 5a). As shown in Figure 5b,c, a large number of biggish Al6Mn phases (its average length is about 50 nm, and length-diameter ratio is about 1.5) and small oval η′ phases (its size is about 5 nm) are diffusely distributed in the grains. Compared to T6 alloy, the size and shape of η′ phases in 300°C4P-T6 alloy after ECAP extrusion did not change significantly, but the Al6Mn phases became finer in size and changed from a short rod-like shape to an elliptical shape (its length-diameter ratio reduces). A small amount of Al6Mn phases also appear at the grain boundaries of 300°C4P-T6 alloy (Figure 5a).

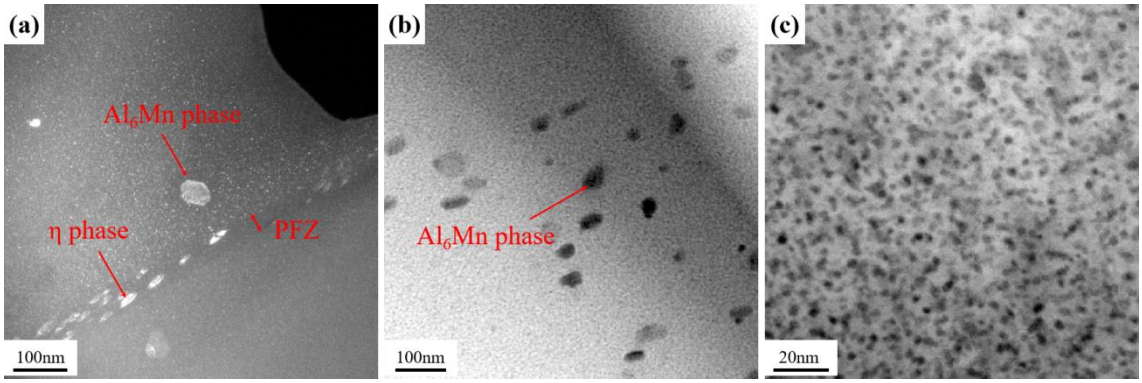

Figure 5. Typical precipitates of 300℃4P-T6 alloy observed by TEM: (a) along grain boundaries; (b, c) inside grains.

Figure 6 shows the three typical precipitates in 300℃4P-R80%-T6 alloy. As compared Figure 6a with Figure 5a, the continuous distributed η phases at the grain boundaries of 300℃4P-R80%-T6 alloy becomes more elongated compared to that of 300°C4P-T6 alloy, with the average length increasing

 doi:10.20944/preprints202408.1587.v1

to 55 nm and the average width decreasing to 18 nm (a length-diameter ratio of approximately 3). The width of the PFZ at the grain boundaries of the 300℃4P-R80%-T6 alloy (the average width is about 40 nm) doesn't change too much compared to that of 300℃4P-T6 alloy. The biggish Al6Mn phases and small η' phases are abundantly distributed within the grains, as shown in Figure 6b,c. The average length of the Al6Mn phase is about 48 nm with a length-diameter ratio of 1.4, which is slightly smaller than the size of the Al6Mn phases in 300℃4P-T6 alloy. The average length of the η' phases is also about 5 nm.

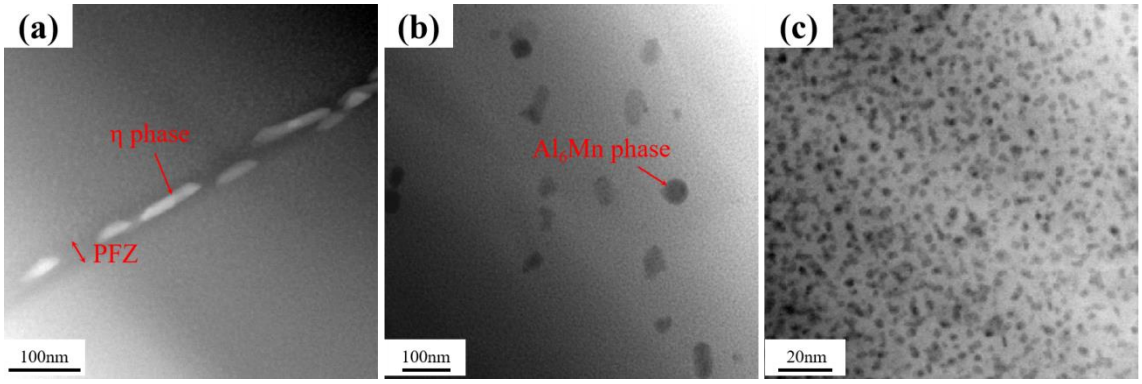

Figure 6. TEM images of 300℃4P-R80%-T6 alloy: (a) along grain boundaries; (b, c) inside grains.

In order to exhibits the distribution of typical Al6Mn precipitates of 7046 alloy in a greater range, Figure 7 is presented. As shown in Figure 7a, T6 alloy is littered with short rod-like Al6Mn phases with a large size (its average length is about 102 nm, and length-diameter ratio is about 2.6). After ECAP extrusion, the Al6Mn phases in 300℃4P-T6 alloy becomes finer and the shape changes from short rod-like to elliptical (its average length is about 50 nm, and length-diameter ratio reduces to 1.5). The quantity of the Al6Mn phases in 300℃4P-T6 alloy do not change a lot, but the distribution of them become more uniform (Figure 7b). 300℃4P-R80%-T6 alloy have a significantly higher content of Al6Mn phases and are similar in size and shape compared to 300℃4P-T6 alloy's (Figure 7c).

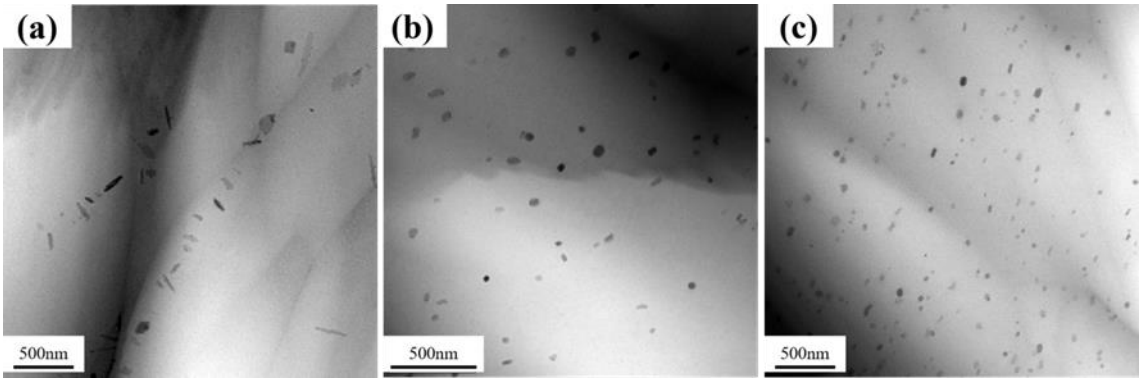

Figure 7. Typical Al6Mn precipitates of 7046 alloy observed by TEM: (a) T6; (b) 300℃4P-T6; (c) 300℃4P-R80%-T6.

3.2. Mechanical Properties

Typical engineering stress-strain curves of as-cast, T6, R80%-T6, 300°C4P-T6 and 300°C4P-R80%-T6 alloys are shown in Figure 8. The as-cast alloy exhibits a UTS of 273 MPa, a YS of 203 MPa and an EL of 5.0%. After T6 treatment, the alloy shows an increase in the UTS and YS and a decrease in the EL. It presents a UTS of 409 MPa, a YS of 357 MPa, and an EL of 4.0%. By pre-rolling treatment, R80%-T6 alloy shows a slight increase in YS and a significant increase in UTS and EL, with a UTS, YS and EL of 462 MPa, 365 MPa and 15.6% respectively. The strengthening and toughening effect of pre-ECAP treatment is more obvious. The UTS, YS and EL of 300°C4P-T6 alloy are 485 MPa, 366 MPa and 19.0% respectively. The mechanical properties of the alloy are further improved by the additional RT

 doi:10.20944/preprints202408.1587.v1

rolling process. 300°C4P-R80%-T6 alloy shows a UTS, YS and EL of 508 MPa, 393 MPa and 23.4%, higher than that of T6 alloy by 24.2%, 10.1% and 485%, respectively. The UTS, YS and EL of these alloys are given in Table 2.

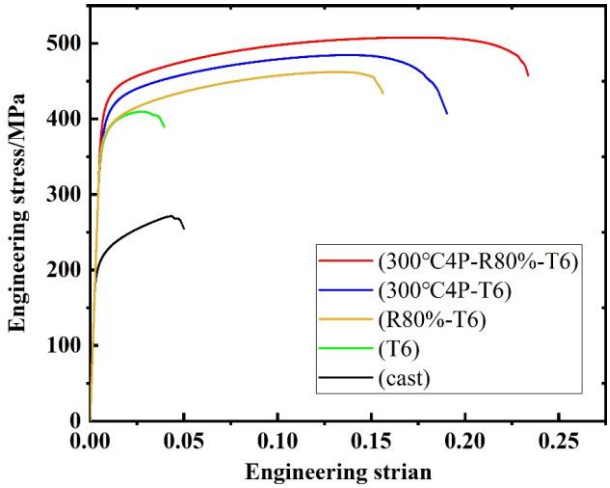

Figure 8. Typical Engineering stress-strain curves of the studied alloys.

Table 2. Summary of the mechanical properties of the as-cast, T6, R80%-T6, 300℃4P-T6 and 300℃4P-R80%-T6 alloys.

Alloy	UTS(MPa)	YS(MPa)	EL(%)
as-cast	~272	~203	~5.0
T6	~409	~357	~4.0
R80%-T6	~462	~365	~15.6
300℃4P-T6	~485	~366	~19.0
300℃4P-R80%-T6	~508	~393	~23.4

3.3. Tensile Fracture Surfaces

Figure 9 shows the tensile fractures surfaces of the 7046 alloy after different processes. Some dimples present in the fracture surfaces of as-cast alloys, but the dimples are large and there are some cleavage steps in local, as can be seen in Figure 9a. A tract of cleavage steps are observed in T6 alloys, and the dimples are barely observed (Figure 9b), making it an obvious brittle fracture. Performing ECAP extrusion prior to T6 treatment, a large number of small sized dimples are nested between the large icing sugar-like patterns (Figure 9c), which correspond to an increase in the ductility of 300℃4P-T6 alloy. Performing ECAP and RT rolling prior to T6 treatment, the dimples become deeper, the size of them is smaller and the amount of them increases, transforming it into a ductile fracture (Figure 9d). These fracture characteristics correspond to a good EL% (23.4%) of 300℃4P-R80%-T6 alloy.

 doi:10.20944/preprints202408.1587.v1

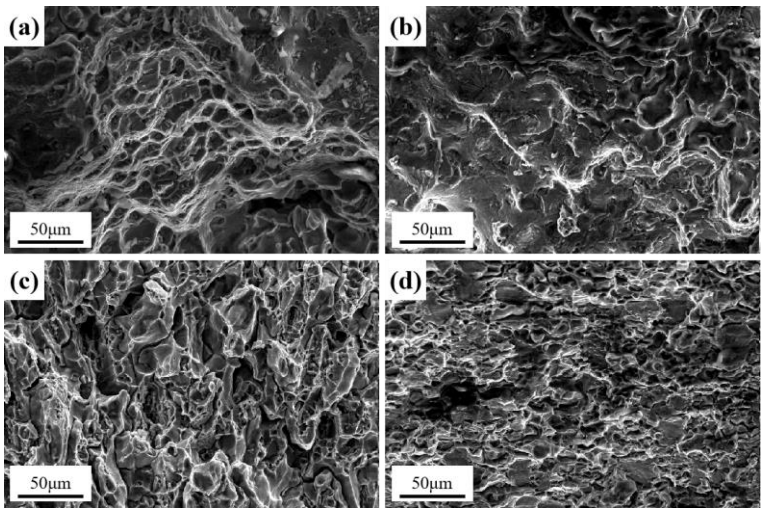

Figure 9. SEM of the tensile fractures surfaces of 7046 alloy: (a) as-cast; (b) T6; (c) 300℃4P-T6; (d) 300 ℃4P-R80%-T6.

4. Discussion

As demonstrated in the above section, 300°C4P-R80%-T6 alloy developed in this work exhibits excellent mechanical properties, which indicates that perform ECAP and RT rolling prior to T6 treatment can greatly improve the mechanical properties of the alloy. In this section, the strengthening and toughening mechanisms of 300°C4P-T6 and 300°C4P-R80%-T6 alloys are discussed.

4.1. Strengthening Mechanism

T6 treatment slightly decreases the ductility but greatly enhances the strength. To be specific, the UTS of T6 alloy increases to 409 MPa, which is about 50% higher than that of as-cast alloy (272 MPa). It can be reasonably concluded that the UTS increment (409-272=137 MPa) of the T6 alloy mainly contributed from the η' precipitates (i.e. the second phase strengthening). When it comes to 300°C4P-T6 and T6 alloys, the UTS increases about 76 MPa. The main strategies to improve the mechanical properties are (ⅰ) solid solution strengthening, (ⅱ) fine-grain strengthening, (ⅲ) second phase strengthening and (ⅳ) dislocation strengthening [41]. In this study, all the samples after different processes were subjected to T6 treatment, which eliminates the internal stresses and a large number of strengthening phases precipitate. Dislocation entanglements can hardly be observed, and the textures are weak (Figure 3). Consequently, the contribution of dislocation strengthening and solid solution strengthening can be neglected. Fine-grain strengthening can be calculated by the Hall-Petch relation [21,42], as shown in Eq. (1)

$$\sigma_{HP} = \sigma_0 + kd^{-1/2} \tag{1}$$

where σ_0 denotes the lattice friction stress, k is the Hall-Petch slope and d is the average grain size. As can be seen from Eq. (1), fine-grain strengthening depends on the grain refinement. The AGS of T6 alloy is about 265 μm (Figure 2d). Performing 300°C 4P-ECAP before T6 treatment, the AGS of 300°C4P-T6 alloy rapidly drops to 40 μm (Figure 2f), which implies that fine-grain strengthening does contribute to a partial increase in strength.

Second phase strengthening is generally considered to be controlled by the Orowan mechanism [43]. It can be calculated by

$$\sigma_s = \frac{0.13Gb}{\lambda} ln \frac{d_s}{2b} \tag{2}$$

where G denotes the shear modulus of Al, b is the Burgers vector for basal slip of Al, λ is the average interparticle spacing and d_s is the average particle size. As can be seen from Eq. (2), second phase strengthening depends on the size and distribution of the precipitates. There are three typical

 doi:10.20944/preprints202408.1587.v1

precipitates (η phase, Al6Mn phase and η' phase) along the grain boundaries and inside the grains of T6 and 300°C4P-T6 alloys (Figures 4 and 5). Firstly, the η phases with a large dimensional difference are observed at the grain boundaries in T6 alloy, with length dimensions ranging from approximately 30 nm to 450 nm and length-diameter ratios ranging from 1.6 to 5.1, as shown in Figure 4a,b. The size distribution of the η phases of 300℃4P-T6 alloy at the grain boundaries is more uniform and finer than that of T6 alloy, with an average length size of about 38 nm and a length-diameter ratio of about 2.7 (Figure 5a). Secondly, Al6Mn phases precipitates inside the grains of T6 alloy have an average length about 102 nm, and a length-diameter ratio about 2.6 (Figure 4c). When it comes to 300°C4P-T6 alloy, the average length of Al6Mn phases reduces to 50 nm, and their morphology changes from short rod-like to elliptical (Figure 5b). Both the average interparticle spacing of η phases and Al6Mn phases in T6 and 300°C4P-T6 alloys are much larger than the average particle size of them. According to Eq. (2), the strengthening contribution of η phases and Al6Mn phases is so limited. Thirdly, the η' phases are the main strengthening phases in the present studied alloys [4,44], which have the similar size in both T6 and 300°C4P-T6 alloys (Figures 4d and 5c). Therefore, the strengthening contribution from η' phases depends on their quantity. The quantity of η' phases can hardly be compared directly, while it can indirectly be realized by comparing the width of PFZ. As the solute depletion is one of the main reasons for the occurring of PFZ [45,46], η phases nucleate first at grain boundaries by drawing the solutes from the nearby matrix, leading to the occurring of PFZs close to the grain boundaries [45]. So, the more or coarser η phases appear along the grain boundaries, the wider the PFZ becomes. Meanwhile, it is known that the η phases and η' phases are composed of the same elements (both are MgZn2) and the chemical composition is identical in the present studied alloy. Consequently, it can be roughly estimated that the wider the PFZ there is, the more or coarser η phases there are, and the fewer η' phases there will be. The average width of PFZ in T6 alloy is about 150 nm (Figure 4a,b), while that in the 300°C4P-T6 alloy significantly reduces to 44 nm (Figure 5a). Therefore, it can be deduced that the number of η' phases are much more in 300°C4P-T6 alloy than that in T6 alloy.

As the composition of precipitates is different with the matrix, the solute atoms must both find vacancies and have enough energy to move into the vacant site to complete the diffusely distribution of η' phases in grains [47]. Meanwhile, the precipitate nucleation rate reaches the maximum at HT, and the nucleation and growth of precipitates are always competitive with each other, which causes some η' phases transformed into η phases [48] and makes the primary strengthening η' phases hopeless to reach the maximum density. The HT ECAP prior to T6 treatment actually increases the concentration of vacancies and provide more strain energy [49]. During ECAP extrusion, the growth of small precipitates will be inhibited, and basically no small platelets have the ability to grow into larger precipitates. The growth of large precipitates is mainly through coalescence rather than through the dissolution of small precipitates. The higher concentration of vacancies and more strain energy help the further precipitation of small η' phases, and prevent them from transforming into large η phases. That's why there are much more η' phases in 300°C4P-T6 alloy than in T6 alloy.

Above all of these, the higher strength of 300°C4P-T6 alloy can be attributed to the combination of the fine-grain strengthening and the second phase strengthening by more η' phases.

The strengthening of the alloy is further improved by the additional RT rolling process after ECAP and before T6 treatment. The grain size of 300°C4P-R80%-T6 alloy is further refined with an AGS of 19 μm (Figure 2h). The average width of PFZ in 300°C4P-R80%-T6 alloy (40 nm) is similar with that in 300°C4P-T6 alloy (Figures 5a and 6a), which means that the η' phases in 300°C4P-R80%-T6 alloy are equivalent to those in 300°C4P-T6 alloy. The second phase strengthening of them is almost the same. Therefore, the further increase in the strength of 300°C4P-R80%-T6 alloy is mainly due to the fine-grain strengthening.

4.2. Toughening Mechanism

By pre-ECAP treatment, 300°C4P-T6 alloy exhibits an EL of 23.7%, exhibiting an improvement of 485% compared to that of T6 alloy. The plasticity of the alloy is affected by a series of microstructure characteristics, including the crystal structure (grain size and orientation), coarse intermetallic

 doi:10.20944/preprints202408.1587.v1

phases, PFZ and precipitates in grains and at the grain boundaries [13,50,51]. Fine-grain strengthening is a strengthening mechanism that can increase both plasticity and strength [52]. When compared to that of T6 alloy (265 μm), the AGS of 300°C4P-T6 alloy sharply reduces to 40 μm (Figure 2d,f). In this study, excepting for increasing the UTS and YS of the alloy, fine-grain strengthening also significantly increases the plasticity of the alloy.

The coarse intermetallic phases have an adverse effect on the plasticity of the alloy as they are usually the source of voids/cracks [53]. As shown in Figure 1b, the coarse intermetallic phases (mainly are Al7Cu2Fe phases) in T6 alloy are large in size and distributed unevenly. Performing 4 passes of ECAP at 300℃ prior to T6 treatment, the coarse intermetallic phases become finer and distributed diffusely due to the fragmentation (Figure 1c), which is conducive to improving the plasticity of the alloy.

In addition, by comparing Figure 5a with Figure 4a,b, it can be seen that pre-ECAP results in a significant reduction in the width of PFZ. The width of the PFZ at the grain boundaries of 300°C4P-T6 alloy is significantly reduced to 44 nm (Figure 5a). PFZs distributed along the grain boundaries are much softer than the matrix. The preferential deformation of PFZs during deformation leads to the accumulation of dislocations and the concentration of stress, gradually microcracks nucleate at the interface of the PFZ and the matrix, which are detrimental to the plasticity of alloys [54,55]. With the PFZs refining, the negative influence on the plasticity will diminish.

As plastic deformation proceeds, coarse grain boundary precipitates (GBPs) are usually the source of voids/cracks, leading to intergranular fractures and a significant reduction in plasticity [45]. The size of the GBP η phases of 300℃4P-T6 alloy is more uniform and finer than that of T6 alloy, with an average length of about 38 nm and a length-diameter ratio of about 2.7 (Figure 5a). The refinement of GBP η phases also contributes to the higher plasticity of 300°C4P-T6 alloy.

Besides, there are a considerable number of nano-sized A16Mn precipitates in the grains, which are finer and elliptical in the 300°C4P-T6 alloy (Figure 7a and 7b). During the deformation, once the dislocation is blocked by the A16Mn precipitates, it tends to change the slip system by means of cross-slip. This cross-slip allows the deformation to maintain uniformly good plasticity [56,57]. Above all of these, the high plasticity of 300°C4P-T6 alloy can mainly be attributed to the grain refinement and the optimization of the size and shape of Al6Mn phases. The fragmentation of the coarse intermetallic phases and the refinement of GBP η phases and PFZs diminish the negative influence on the plasticity.

When it comes to 300°C4P-R80%-T6 and 300°C4P-T6 alloys, the EL further increases from 19% to 23.4%. The grain size of 300°C4P-R80%-T6 alloy is further refined with an AGS of 19 μm (Figure 2h), leading to fine-grain strengthening. The coarse intermetallic phases (Al7Cu2Fe phases) in 300°C4P-T6 and 300°C4P-R80%-T6 alloys are all fragmented in small size and diffusely distributed (Figure 1c,d). The width of the PFZs in 300°C4P-R80%-T6 alloy are similar to those in 300°C4P-T6 alloy (Figure 5a and 6a). The distribution and the size of η and η' phases are almost the same, as compared Figure 5a,c with Figure 6a,c. But the quantity of the Al6Mn precipitates in 300°C4P-R80%-T6 alloy are much more than that in 300°C4P-T6 alloy.

It is generally accepted that the transition temperature of Al6Mn phases can be reduced by ECAP extrusion, which is closely related to the strain energy accumulated within the material as the number of passes increased [58]. The dislocation formed during the severe plastic deformation increases the strain energy and this can be expressed in the following equation

$$E_{stored} = Gb^2 \frac{\rho}{4\pi\kappa} In(b\sqrt{\rho}) \quad (3)$$

Where, G is the shear modulus of Al, b is the Burgers vector for basal slip of Al, κ is arithmetic average of 1 and (1-ν), ρ is dislocation density and ν is Poisson ratio. Eq. (3) is controlled by ρ, the greater the ρ is, the greater the strain energy will be. For 300℃4P and 300℃4P-R80% alloys, the dislocation density increases as the increase of accumulation of plastic deformation, the strain energy increases, and the precipitation temperature for Al6Mn phase decreases, making it easier to precipitate. This is consistent with the observation that 300℃4P-R80%-T6 alloy has a greater number of finer and elliptical Al6Mn phases. 300℃4P-R80%-T6 alloy has a significantly higher content of

 doi:10.20944/preprints202408.1587.v1

Al6Mn phases and are similar in size and shape compared to 300℃4P-T6 alloy's. Therefore, the further increase in plasticity of 300℃4P-R80%-T6 alloy is mainly due to the grain refinement and the more number of fine Al6Mn precipitates.

5. Conclusions

In this study, 7046 aluminum alloy with high strength and excellent ductility were prepared by 4 passes of ECAP, RT rolling and T6 treatment. Based on the findings from this study, we conclude the following:

(1) 7046 aluminum alloy processed by 4 passes of HT ECAP prior to T6 treatment realizes an obvious improvement in both strength and ductility, with UTS of 485 MPa, YS of 366 MPa and EL of 19%, respectively. The mechanical properties of the alloy are further improved by the additional RT rolling process, with a UTS, YS and EL of 508 MPa, 393 MPa and 23.4%, exceeding that of T6 alloy by 24.2%, 10.1% and 485%, respectively.

(2) Strength enhancement for the 300℃4P-T6 and 300℃4P-R80%-T6 alloys is attributed to the combination of the fine-grain strengthening and the second phase strengthening by more η' phases.

(3) The higher plasticity of 300℃4P-R80%-T6 and 300°C4P-T6 alloys compared to T6 alloy can mainly be attributed to the grain refinement and the optimization of the size and shape of Al6Mn phases. The fragmentation of the coarse intermetallic phases and the refinement of GBP η phases and PFZs diminish the negative influence on the plasticity.

(4) There are more precipitates of η' and Al6Mn phases in the 300℃4P-R80%-T6 and 300°C4P-T6 alloys, which are the main reasons for SPD process enhancing the strengthening and toughening effect of T6 treated 7046 aluminum alloy.

Author Contributions: Yuna Wu: Conceptualization, Methodology, Writing - review & editing, Funding acquisition. **Hongchen Dong**: Data curation, Writing - original draft. **Hao Huang**: Conceptualization, Investigation. **Ting Yuan**: Methodology, Funding acquisition. **Jing Bai**: Conceptualization, Methodology, Funding acquisition. **Jinghua Jiang**: Methodology, Supervision. **Feng Fang**: Conceptualization, Writing - review & editing. **Aibin Ma**: Conceptualization, Supervision.

Data Availability Statement: The data that support the findings of this study are available on request from the corresponding author.

Acknowledgments: The authors would like to acknowledge the financial supports of the Fundamental Research Funds for the National Natural Science Foundation of China (52303390), the Fundamental Research Funds for the Central Universities (B230201002), the China Postdoctoral Science Foundation (2021M690860), Jiangsu Provincial Key Research and Development Program (BE2021027), and Suzhou Science and Technology Project (SJC2023005, SZS2023023).

Conflicts of Interest: The authors declare that they have no known competing financial interests or personal relationships that could have appeared to influence the work reported in this paper.

References

1. Chen Y, Wu Y, Geng J, et al. Pre-precipitating promoted by microshear bands effectively circumvents strength-ductility trade-off of RT-rolled Al-6Zn-1Mg alloy [J]. Journal of Materials Research and Technology, 2024, 28: 2767-77.
2. Zhao Y, Tian T, Jia H, et al. Effects of Mg/Zn ratio and pre-aging on microstructure and mechanical properties of Al-Mg-Zn-Cu alloys [J]. Journal of Materials Research and Technology, 2023, 27: 1874-85.
3. Shin J, Kim T, Kim D, et al. Castability and mechanical properties of new 7xxx aluminum alloys for automotive chassis/body applications [J]. Journal of Alloys and Compounds, 2017, 698: 577-90.
4. Azarniya A, Taheri A K, Taheri K K. Recent advances in ageing of 7xxx series aluminum alloys: A physical metallurgy perspective [J]. Journal of Alloys and Compounds, 2019, 781: 945-83.
5. Jiang K-D, Zhang Z, Zhu W-B, et al. Influence of V additions on microstructures, tensile and fatigue properties of Al-Zn-Mg alloys [J]. Materials Science and Engineering: A, 2022, 829: 142184.
6. Deng Y, Peng B, Xu G, et al. Effects of Sc and Zr on mechanical property and microstructure of tungsten inert gas and friction stir welded aerospace high strength Al-Zn-Mg alloys [J]. Materials Science and Engineering: A, 2015, 639: 500-13.

7. Wang S-S, Huang I-W, Yang L, et al. Effect of Cu content and aging conditions on pitting corrosion damage of 7xxx series aluminum alloys [J]. Journal of the Electrochemical Society, 2015, 162(4): C150.
8. Hattori C, Almeida G, Gonçalves R, et al. Microstructure and fatigue properties of extruded aluminum alloys 7046 and 7108 for automotive applications [J]. Journal of Materials Research and Technology, 2021, 14: 2970-81.
9. He D, Chen S-b, Lin Y C, et al. Microstructural evolution characteristics and a unified dislocation-density related constitutive model for a 7046 aluminum alloy during hot tensile [J]. Journal of Materials Research and Technology, 2023, 25: 2353-67.
10. Jiang F, Huang J, Jiang Y, et al. Effects of quenching rate and over-aging on microstructures, mechanical properties and corrosion resistance of an Al–Zn–Mg (7046A) alloy [J]. Journal of Alloys and Compounds, 2021, 854: 157272.
11. Shah S, Thronsen E, Hatzoglou C, et al. Effect of cyclic ageing on the early-stage clustering in Al-Zn-Mg (-Cu) alloys [J]. Materials Science and Engineering: A, 2022, 846: 143280.
12. Shah S, Gopal A, Thronsen E, et al. Precipitation, mechanical properties and early slant ductile fracture in cyclic and naturally aged Al-Zn-Mg (-Cu) alloys [J]. Materials & Design, 2022, 222: 111026.
13. Qiu Y, Li X, Huang H, et al. Effects of ultrasonic vibration on the microstructure and corrosion properties of the 7046 Al alloy [J]. Vacuum, 2022, 205.
14. Oger L, Lafouresse M C, Odemer G, et al. Hydrogen diffusion and trapping in a low copper 7xxx aluminium alloy investigated by Scanning Kelvin Probe Force Microscopy [J]. Materials Science and Engineering: A, 2017, 706: 126-35.
15. Liao Z, Li C, Liu S, et al. Effect of post aging on mechanical properties of friction stir welded 7046 aluminum alloy [J]. Chinese Journal of Materials Research, 2021, 35(7): 543-52.
16. Yang M, Li C, Liu S, et al. Effect of Artificial Aging on Microstructure and Mechanical Properties of Friction Stir Welded Joint of 7003/7046 Al-alloys [J]. Chinese Journal of Materials Research, 2020, 34(7): 495-504.
17. Yu Z, Jin S, Feng M, et al. Temperature-dependent-composition of η phase in an Al-Zn-Mg-Cu alloy under high pressure torsion: Kinetics and thermodynamics [J]. Acta Materialia, 2022, 237: 118181.
18. Deschamps A, Hutchinson C. Precipitation kinetics in metallic alloys: Experiments and modeling [J]. Acta Materialia, 2021, 220: 117338.
19. Rometsch P A, Zhang Y, Knight S. Heat treatment of 7xxx series aluminium alloys—Some recent developments [J]. Transactions of Nonferrous Metals Society of China, 2014, 24(7): 2003-17.
20. Hou Y, Chen L, Li Z, et al. Effects of artificial aging on microstructure, mechanical properties and stress corrosion cracking of a novel high strength 7A99 Al alloy [J]. Materials Science and Engineering: A, 2020, 780: 139217.
21. Ma K, Wen H, Hu T, et al. Mechanical behavior and strengthening mechanisms in ultrafine grain precipitation-strengthened aluminum alloy [J]. Acta Materialia, 2014, 62: 141-55.
22. Zou Y, Cao L, Wu X, et al. Unusual secondary precipitation within the primary precipitation free zone substantially enhances the ductility of Al-Zn-Mg-Cu alloy [J]. Materials Science and Engineering: A, 2023, 881: 145384.
23. Chen Z, Yuan Z, Ren J. The mechanism of comprehensive properties enhancement in Al-Zn-Mg-Cu alloy via novel thermomechanical treatment [J]. Journal of Alloys and Compounds, 2020, 828: 154446.
24. Afifi M A, Wang Y C, Pereira P H R, et al. Effect of heat treatments on the microstructures and tensile properties of an ultrafine-grained Al-Zn-Mg alloy processed by ECAP [J]. Journal of Alloys and Compounds, 2018, 749: 567-74.
25. Tański T, Snopiński P, Pakieła W, et al. Structure and properties of AlMg alloy after combination of ECAP and post-ECAP ageing [J]. Archives of Civil and Mechanical Engineering, 2016, 16: 325-34.
26. Yuan Y, Ma A, Jiang J, et al. Optimizing the strength and ductility of AZ91 Mg alloy by ECAP and subsequent aging [J]. Materials Science and Engineering: A, 2013, 588: 329-34.
27. Wang W, Pan Q, Wang X, et al. Mechanical properties and microstructure evolution of ultra-high strength Al-Zn-Mg-Cu alloy processed by room temperature ECAP with post aging [J]. Materials Science and Engineering: A, 2018, 731: 195-208.
28. Chen X, Xia D, Zhang J, et al. Ultrafine-grained Al-Zn-Mg-Cu alloy processed via cross accumulative extrusion bonding and subsequent aging: Microstructure and mechanical properties [J]. Journal of Alloys and Compounds, 2020, 846: 156306.
29. Yu Z, Xu X, Mansoor A, et al. Precipitate characteristics and their effects on the mechanical properties of as-extruded Mg-Gd-Li-Y-Zn alloy [J]. Journal of Materials Science & Technology, 2021, 88: 21-35.
30. Ren J, Wang R, Peng C, et al. Multistage aging treatment influenced precipitate characteristics improve mechanical and corrosion properties in powder hot-extruded 7055 Al alloy [J]. Materials Characterization, 2020, 170: 110683.
31. Dai P, Luo X, Yang Y, et al. Nano-scale precipitate evolution and mechanical properties of 7085 aluminum alloy during thermal exposure [J]. Materials Science and Engineering: A, 2018, 729: 411-22.

32. Sha G, Wang Y, Liao X, et al. Influence of equal-channel angular pressing on precipitation in an Al–Zn–Mg–Cu alloy [J]. Acta Materialia, 2009, 57(10): 3123-32.
33. Chinh N Q, Gubicza J, Czeppe T, et al. Developing a strategy for the processing of age-hardenable alloys by ECAP at room temperature [J]. Materials Science and Engineering: A, 2009, 516(1-2): 248-52.
34. Cardoso K, Travessa D, Botta W, et al. High Strength AA7050 Al alloy processed by ECAP: Microstructure and mechanical properties [J]. Materials Science and Engineering: A, 2011, 528(18): 5804-11.
35. Shaeri M, Shaeri M, Ebrahimi M, et al. Effect of ECAP temperature on microstructure and mechanical properties of Al–Zn–Mg–Cu alloy [J]. Progress in Natural Science: Materials International, 2016, 26(2): 182-91.
36. Zuo J, Hou L, Shi J, et al. The mechanism of grain refinement and plasticity enhancement by an improved thermomechanical treatment of 7055 Al alloy [J]. Materials Science and Engineering: A, 2017, 702: 42-52.
37. Sun C, Liu H, Xu Z, et al. Refining 18R-LPSO phase into sub-micron range by pre-kinking design and its prominent strengthening effect on Mg97Y2Zn1 alloy [J]. Journal of Materials Science & Technology, 2024, 176: 13-24.
38. Chen Y, Wu Y, Li Y, et al. RT ECAP and rolling bestow high strength and good ductility on a low lithium aluminum alloy [J]. Journal of Materials Research and Technology, 2023, 25: 5561-74.
39. Yuan T, Jiang J, Ma A, et al. Simultaneously improving the strength and ductility of an Al-5.5Mg-1.6Li-0.1Zr alloy via warm multi-pass ECAP [J]. Materials Characterization, 2019, 151: 530-41.
40. Wang X, Pan Q, Liu L, et al. Characterization of hot extrusion and heat treatment on mechanical properties in a spray formed ultra-high strength Al-Zn-Mg-Cu alloy [J]. Materials Characterization, 2018, 144: 131-40.
41. Wu Y, Liao H, Lü C. Dynamic precipitation and recrystallization in Al-12.5 wt% Si-0.6 wt% Mg-0.1 wt% Ti alloy during hot-rolling and their impacts on mechanical properties [J]. Journal of Alloys and Compounds, 2019, 788: 125-35.
42. Cordero Z C, Knight B E, Schuh C A. Six decades of the Hall–Petch effect–a survey of grain-size strengthening studies on pure metals [J]. International Materials Reviews, 2016, 61(8): 495-512.
43. Sun W, Qiao X, Zheng M, et al. Altered ageing behaviour of a nanostructured Mg-8.2 Gd-3.8 Y-1.0 Zn-0.4 Zr alloy processed by high pressure torsion [J]. Acta Materialia, 2018, 151: 260-70.
44. Won S-J, So H, Kang L, et al. Development of a high-strength Al-Zn-Mg-Cu-based alloy via multi-strengthening mechanisms [J]. Scripta Materialia, 2021, 205: 114216.
45. Zindal A, Jain J, Prasad R, et al. Effect of heat treatment variables on the formation of precipitate free zones (PFZs) in Mg-8Al-0.5 Zn alloy [J]. Materials Characterization, 2018, 136: 175-82.
46. Zhao H, De Geuser F, Kwiatkowski da Silva A, et al. Segregation assisted grain boundary precipitation in a model Al-Zn-Mg-Cu alloy [J]. Acta Materialia, 2018, 156: 318-29.
47. Sun W, Zhu Y, Marceau R, et al. Precipitation strengthening of aluminum alloys by room-temperature cyclic plasticity [J]. Science, 2019, 363(6430): 972-5.
48. Sha G, Wang Y B, Liao X Z, et al. Influence of equal-channel angular pressing on precipitation in an Al-Zn-Mg-Cu alloy [J]. Acta Materialia, 2009, 57(10): 3123-32.
49. Chung T-F, Yang Y-L, Huang B-M, et al. Transmission electron microscopy investigation of separated nucleation and in-situ nucleation in AA7050 aluminium alloy [J]. Acta Materialia, 2018, 149: 377-87.
50. Li B, Wang X, Chen H, et al. Influence of heat treatment on the strength and fracture toughness of 7N01 aluminum alloy [J]. Journal of Alloys and Compounds, 2016, 678: 160-6.
51. Han N, Zhang X, Liu S, et al. Effects of pre-stretching and ageing on the strength and fracture toughness of aluminum alloy 7050 [J]. Materials Science and Engineering: A, 2011, 528(10-11): 3714-21.
52. Tang L, Peng X-y, Jiang F-q, et al. Strong and ductile Al-Zn-Mg-Zr alloy obtained by equal angular pressing and subsequent aging [J]. Transactions of Nonferrous Metals Society of China, 2022, 32(5): 1428-41.
53. Cvijović Z, Rakin M, Vratnica M, et al. Microstructural dependence of fracture toughness in high-strength 7000 forging alloys [J]. Engineering Fracture Mechanics, 2008, 75(8): 2115-29.
54. Ogura T, Hirosawa S, Sato T. Quantitative characterization of precipitate free zones in Al-Zn-Mg (-Ag) alloys by microchemical analysis and nanoindentation measurement [J]. Science and Technology of Advanced Materials, 2004, 5(4): 491-6.
55. Ogura T, Hirose A, Sato T. Effect of PFZ and grain boundary precipitate on mechanical properties and fracture morphologies in Al-Zn-Mg (Ag) alloys; proceedings of the Materials Science Forum, F, 2010 [C]. Trans Tech Publ.
56. Shen W, Hu A, Liu S, et al. Al-Mn Alloys for Electrical Applications: A Review [J]. Journal of Alloys and Metallurgical Systems, 2023: 100008.
57. Nikulin I, Kipelova A, Malopheyev S, et al. Effect of second phase particles on grain refinement during equal-channel angular pressing of an Al-Mg-Mn alloy [J]. Acta Materialia, 2012, 60(2): 487-97.
58. Lee J C, Lee S H, Kim S W, et al. The thermal behavior of aluminum 5083 alloys deformed by equal channel angular pressing [J]. Thermochimica acta, 2010, 499(1-2): 100-5.

 doi:10.20944/preprints202408.1587.v1